Erik Jonsson School of Engineering and Computer Science

2014-03

Artificial Heart for Humanoid Robot

UTD Author(s): Akshay Potnuru, Lianjun Wu and Yonas Tadesse

Potnuru, Akshay, Lianjun Wu, and Yonas Tadesse. 2014. "Artificial heart for humanoid robot." Electroactive Polymer Actuators And Devices (eapad) 2014 9056: 90562F-1 to -16.

Artificial heart for humanoid robot

Akshay Potnuru, Lianjun Wu and Yonas Tadesse [*a]

[a] Department of Mechanical Engineering, University of Texas at Dallas, Richardson, TX 75080

ABSTRACT

A soft robotic device inspired by the pumping action of a biological heart is presented in this study. Developing artificial heart to a humanoid robot enables us to make a better biomedical device for ultimate use in humans. As technology continues to become more advanced, the methods in which we implement high performance and biomimetic artificial organs is getting nearer each day. In this paper, we present the design and development of a soft artificial heart that can be used in a humanoid robot and simulate the functions of a human heart using shape memory alloy technology. The robotic heart is designed to pump a blood-like fluid to parts of the robot such as the face to simulate someone blushing or when someone is angry by the use of elastomeric substrates and certain features for the transport of fluids.

Key words: Biomimetic, humanoid, artificial heart, blood flow, shape memory alloy, soft robotics

1. INTRODUCTION

Research on development of artificial hearts for assisting the treatment of patients who are suffering from cardiac failure is being conducted for several decades [1]. The objective of this paper is not to present an artificial heart for humans; rather, it is to discuss the need and implementation of artificial hearts in humanoid robotics to show facial coloration for expression. We will briefly discusses the design of artificial heart that are in use for medical application, the history and existing artificial hearts, the design of shape memory alloys based artificial muscles, humanoid robots with facial expressions(HRwFE) in section 1. Next, we will present a biologically inspired robotic heart that was made of shape memory alloy and silicone elastomer. The design and manufacturing of the robotic heart using rapid prototyping and casting technology will be discussed. The numerical simulation based on finite element analysis and flow simulations of the robotic heart will be presented in section 3. Experimental characterization of the artificial heart will be presented in section 4. Finally, the applications of the robotic heart and conclusions will be discussed.

1.1 Biological Heart

Natural heart is a muscular organ which pumps blood through our body. It is the center of our circulatory system which consists of a network of blood vessels like arteries, veins and capillaries which carry blood to and from of all parts of the body [2]. Research has been done to show how facial color changes are an effective nonverbal communication and also how it plays a significant role in expressing oneself [3]. Human heart plays a significant role in change of facial color as the flow of blood is regulated by the heart to face. The rate of human heart beat per minute plays a important role while expressing emotions like happy, sad, angry and disgust [4]. Facial color change is unique human characteristic which is not shown by other animals even though they possess cardiovascular apparatus which is first observed by Darwin in his studies [5, 6]. Humans mainly show facial coloration for anger, fear and embarrassment. In anger, we show reddening which is caused due to vasodilation, increased contractibility. In fear, we show blanching due to vasoconstriction and in embarrassment we show blushing due to vasodilation [7]. A study in various cultural groups showed that humans connect facial expressions with certain colors [8]. The study showed that anger and happiness are connected to the red color, as in the case naturally we blush for happiness, anger and embarrassment. The green color is connected to disgust and sickness. Naturally these colors are exhibited in humans due to sudden variation in blood pumping to face from heart due to emotional changes experienced which are controlled by the brain. Facial coloration is prominent in specific areas of the face such as the cheeks where the blood vessels are wider in diameter and are nearer to the skin surface, and where there is less reduction of visibility due to tissue fluid [9].

*Corresponding author yonas.tadesse@utdallas.edu

1.2 History and Existing Artificial Hearts

The concept of artificial hearts originated in the 60's after the first heart transplantation in 1967 [10]. The first major breakthrough came out in 1965 where Kolff and Akutsu sustained a calf for almost forty four hours using a pendulum based artificial heart [11]. The first artificial heart transplantation was made in 1969 to Haskell Karp by Cooley and Liotta team where the artificial heart pumped 6 L/min and the patient lived with it for 3 days until a donor heart was available [10]. In 1970 Kolff and Javrik developed Javrik-7 prototype which had two ventricles with air chambers and 6 titanium valves, with attachments to patients arteries [11]. In 1982 Javrik-7 was first implanted in a patient named Barney Clark who survived for 112 days [12]. Later Javrik was renamed as Cardiowest (shown in Figure 1 (a)) and in 2001 Abiomed Inc. began its first Abiocor (shown in Figure 1 (b)) artificial heart implants. The average life of the person after artificial heart was around 50 ± 42 days [13]. The starting models of the artificial heart had technical flaws and the need of huge powers source made them impractical for permanent replacement [14]. This was a major reason for moving the artificial ventricles out of the body and transformed the artificial heart to a ventricular assist device [15].

Cleveland Clinic's continuous-flow total artificial heart is one of the recent input to the science of artificial hearts which has one motor and one rotating assembly supported by a hydrodynamic bearing [16]. A completely simulated 3D thoracic anatomical model with implanted artificial heart was developed for testing and preoperational analysis in Japan [17]. An electromechanically actuated one piece artificial heart which can be completely implanted for permanent human use was developed by Takatani et al [18]. Recently, an artificial heartbeat was developed which mimics the natural heartbeat. The system was actuated by NiTi (SMAs) artificial muscles powered by electrical energy generated by microbial fuel cells (MFC's) like human urine [19]. An anatomically accurate, multi material, patient specific cardiac simulator with sensing and controls was also developed which mimics the functionality of an artificial heart [20].
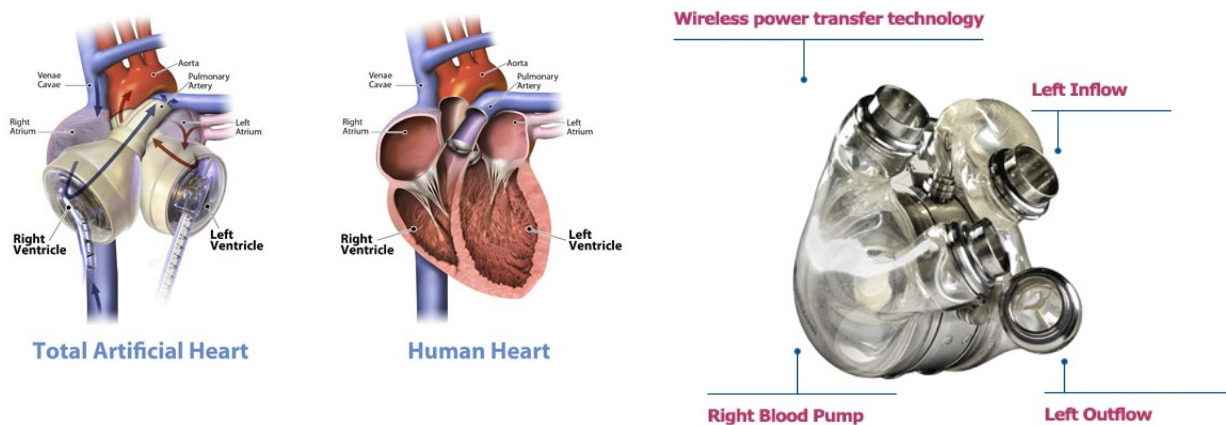

Figure 1: Artificial heart (a) CardioWest™ : Total artificial heart and human heart illustrations with detailed callouts (Courtesy of SynCardia Systems Inc.) [13] and (b) AbioCor®: World's First Artificial Heart (Courtesy of Abiomed Inc.)

1.3 Shape memory alloys artificial muscles

Research on the development of artificial muscles which can mimic natural muscles in performance, size and durability has been growing significantly in recent years due to their unique applications in the design of humanoid robotics and biomimetic systems [21, 22]. There are several kinds of actuators used as artificial muscles such as piezoelectric, electromagnetic, pneumatic, shape memory alloys(SMA) and electro active polymers (EAP) [23]. Shape memory alloys come under smart materials which exhibit super elasticity and shape memory effects. The most widely used alloys in SMA actuators are nickel-titanium, copper-zinc and silver-cadmium at specific compositions. Shape memory effect can be described as the recovery of initial shape after deformation due to residual strain developed in the material by thermal cycling. There are several advantages of shape memory alloys such as: (1) small profiles generally around 100-150 μm in diameter, (2) high force to weight ratio, (3) utilizes simple current drive and (4) silent operation. The maximum operating frequency of SMA is less than 10 Hz which limits its application as of their low operational frequency and narrow bandwidth which is directly proportional to

the time required for heating and cooling of the material [24]. Due to the benefits of SMA, a biologically inspired wet shape memory alloy actuated robotic pump was developed by Matthew et al. [25]. NiTi alloy was tested and showed a potential material to develop artificial muscles which can be used as a cardiac assistance device for dynamic cardiomyoplasty [26]. Nitinol, an alloy of nickel, titanium, cobalt was also considered for actuating as an artificial muscle for the development of an artificial heart [27]. Covalent shaped shape memory alloy fibers were used for creating a senserless control for a sophisticated artificial myocardial contraction by implementing PWM control method [28].

1.4 Humanoid robotics with facial expressions (HRwFE)

Research in androids, autonomous robotics, biomimetic and bionics which include humanoid robotics is being conducted at global scale extensively [29]. Humanoid robotics deals with the study of robots which mimics humans in terms of appearance and functioning. We classified those robots capable of demonstrating facial expression by deforming their face shape as HRwFE. HRwFE is the acronym for humanoid robots with facial expressions. A lot of focus is being given in the research of humanoid robots with facial expressions (HRwFE) which create a foundation in sociable communication between the robot and humans and vice versa [21, 30]. Several HRwFE prototypes were made in the past which include humanoid robot head ROMAN [31], Albert HUBO [32, 33], humanoid robot KOBIAN-R [34], Face Robot SAYA [35], F&Hrobot [36], Geminoid [37], WE-3RIV [38], ER-1 [39], Shape memory alloy based baby head [22]. Some examples are shown in Figure 2. Albert-piezo: ultrasonic motors based humanoid head [40], Lilly humanoid: servo motors and embedded piezoelectric sensors in the face [41] etc. Unique capabilities of humanoids were also presented in the humanoid WE-3RIV [38] which uses facial coloration to show emotions using red EL (Electro Luminescent) thin and light sheet device.

In this paper, we present a method of face color change using a robotic pump and silicone skin having several channels for the flow of blood-like fluid. The sample prototype which will be discussed later is a preliminary work but it can be applicable to the face robots shown in Figure 1. Once the robotic heart is well developed and hollow channels are created within the robots skin, the blood-like fluid can be pumped into the channels and hence change the face color. We used washable colors which are pumped from the artificial heart to demonstrate proof of concepts in a sample skin. Facial expressions and face coloration enables the robots to have unique appearance and have numerous applications. The major applications of humanoid robots with facial applications will be in education institutions as communication person, as a press reporter that can read text effectively, to help people as a receptionist, to teach children with some vocabulary and in psychological rehabilitation for children with Autism [21].
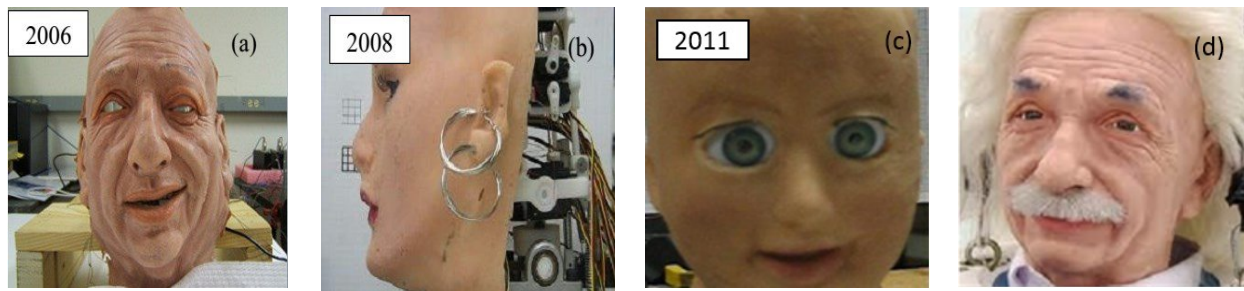

Figure 2. Artificial muscles application humanoids platforms: (a) Albert-piezo: ultrasonic motors based humanoid head, (b) Lilly humanoid: servo motors and embedded piezoelectric sensors in the face, (c) Shape memory alloy based baby head, (d) Albert-HUBO, servo motors based humanoid (Courtesy of Hanson Robotics Inc).

2. DESIGN AND MANUFACTURING

The human heart plays an important role in our metabolic system, which functions as a pump, providing the body with a steady flow of blood by means of regular rhythmic contractions. The heart is located in the mediastinum in the thoracic cavity of the thorax. The outer wall of the heart is composed of three layers, the epicardium, the myocardium which is the muscle of the heart, and the endocardium [42]. The muscle wall of the heart is responsible for pumping the blood through the systemic circulation. When pumping the blood out of the heart, the muscle wall of the heart contracts leading the decrease in the volume of the heart hollow cavity. The contractile elements in a

comparable artificial heart should fulfill the function of the muscle wall of the mammalian heart. Due to the advantages of the shape memory alloy, it is anticipated that the SMA can be used as an efficient contractile element.

2.1 **Biologically inspired design**

The design of the prototype heart is illustrated in Figure 3. The heart is composed of a hollow body which is filled with colored fluid, a soft shell with inlet and outlet ports and a clamp. The material used for fabricating the heart is silicone which enables the heart to have a soft, flexible shell to be compressed by the contraction of the muscle wall. The shape memory alloy fibers (Flexinol® Actuator Wire) are employed as the contractile actuators of the heart. The Flexinol wires have two diameters, 130 and 200 um. The smaller size actuator has less pull force generating ability than the bigger size actuator while the smaller size actuator has quick response due to the less time needed to cool down. The SMA fiber undergoes a phase transformation from martensite phase to austenite phase when thermally activated by electrical current. During the phase transformation, the SMA fibers return to the original length, generating a 'recovery force' which can be harnessed to compress the soft heart. In order to utilize the force generated by SMA fibers upon contraction, six shape memory alloys were anchored in parallel pattern to the exterior of the heart (Fig. 3(a)). The SMA fibers have crimp ends which are attached by screws to one side of the clamp. On the other side of the clamp, small pulleys with a wheel diameter of 6.35 mm were placed. These pulleys help transmit the force generated by the SMA fibers through the body of the heart. Once the SMAs are actuated, the liquid inside of the heart will be forced out from the heart. Since the SMA fibers do not have a completely reversible contraction, a soft sponge consisting of porous material was employed inside of the heart to make the heart return its original shape. Once the electric current is removed from the SMA fibers, they require some time to cool down and relax. Two plastic tubes (internal diameter 2 mm) are attached to the inlet and outlet ports. The wall thickness of the artificial heart is 3 mm. The volume of the artificial heart is 116631 cubic millimeters. Fig. 3 shows the schematic diagram, the CAD model and the sample artificial heart.
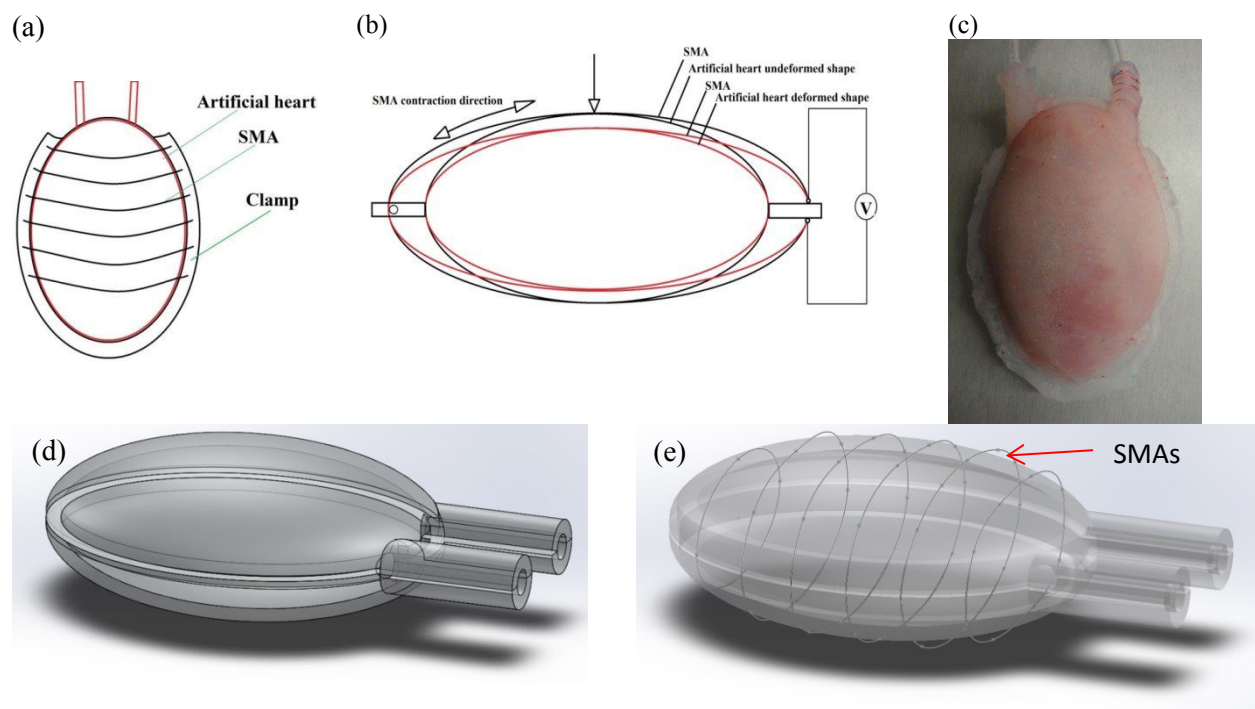

Figure 3. Artificial Heart (a) Schematic diagram of the front view of the artificial heart wrapped with SMA,(b) the section view of the artificial heart and (c) prototype, (d) CAD model and (e) SMA wrapped arround the heart.

2.2 Fabrication

The workflow of the fabrication of the prototype heart is outlined step by step as shown in Figure 4. In order to achieve the aim of our design, a total of four molds were designed in SolidWorks. Then these molds were exported as stl files to be fabricated by 3D printing using Stratasys Dimension Elite 3D printer. 3D printing, also known as an additive manufacturing method, is a rapid prototyping technology which can fabricate a three dimensional object directly from computer-aided design data. While 3D printing has its limitations, 3D printing has several advantages compared with traditional manufacturing methods. Complex shape of the mold can be manufactured using the 3D printer. Another advantage is that 3D printing is time and cost saving for users. These molds are fabricated using ABS plastic rather than metal material that was often used in traditional casting mold method.

After these molds are fabricated, they were assembled to cast elastomer that defines the outline of the artificial heart. Platinum cured silicone rubber (ECOFLEX 0010) was used to fabricate the artificial heart. At first, equal amount of part A and Part B were mixed thoroughly in a beaker for 3 minutes. It is recommended to do the mixing process of vacuum degassing to eliminate the air bubble in the mixture. Since the artificial heart is not for medical usage, it is not required to mix with vacuum chamber. A release agent was sprayed over the molds' surfaces to ensure a smooth demolding. After that procedure, the mixture is poured into the assembled mold slowly and continuously using a syringe in order to get rid of air bubble as much as possible. It took 4 hours for the rubber to cure at room temperature. In step 4, Sil-Poxy silicone adhesive was used to bond the silicone parts together. Finally, the SMA wires were routed around the heart in parallel pattern and the ends of SMA wires were fixed to a clamp. The clamp was designed to provide the SMA wire initial pre-stress.
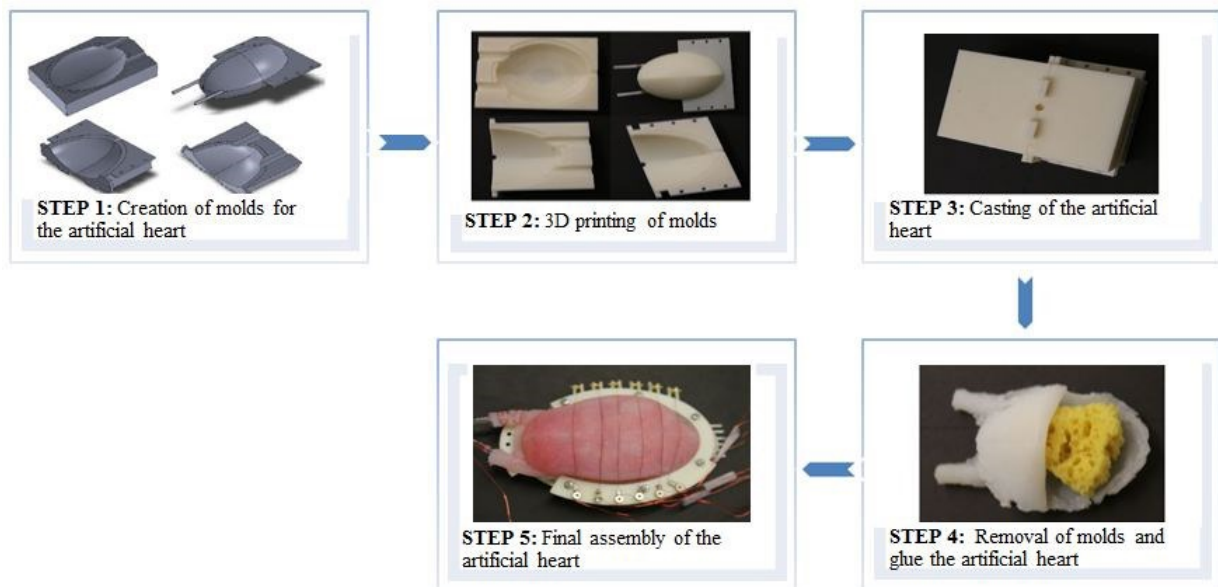

STEP 1: Creation of molds for the artificial heart

STEP 2: 3D printing of molds

STEP 3: Casting of the artificial heart

STEP 5: Final assembly of the artificial heart

STEP 4: Removal of molds and glue the artificial heart

Figure 4. Manufacturing diagram for creation of artifical heart wrapping with SMA fibers

3. MODELING AND SIMULATION

This section describes the computer aided design (CAD) model of the artificial heart using Solidworks[TM] software. A hyperelastic stress analysis simulation is also presented by varying pressure and using the simulation results the volume of the fluid pumped at different pressures is calculated. Lastly, a flow simulation of the fluid flow inside the CAD model is also shown to understand the flow pattern inside the model.

3.1 Computer Aided Design (CAD)

The CAD model of the artificial heart was created using Solidworks 2014 (Dassault Systemes, France). Several iterations were made to arrange shape memory alloy around a silicone body. Initially, one long actuator was made to cover the silicone body in a helically wound manner (Fig.3 (d)). However, a prototype made with such a design did

not provide enough actuation of the artificial heart. We then applied several SMA actuators to run in parallel arrangements as shown in Figure 3(a).

3.2 Hyper elastic Stress Analysis

To calculate the volume of liquid that the heart model can pump using NiTi shape memory alloys, we conducted finite element analysis (FEA) to find the deformation under different pressures. The model material used for the heart model was silicone rubber which has a hyperelastic deformation. The finite element analysis (FEA) simulation was conducted using ABAQUS 6.13 (Dassault Systemes, France) and the hyperelastic simulation was conducted using Mooney–Rivlin model [43, 44].

Mooney–Rivlin model:

Continuum mechanics is a mechanics branch that studies deformation motion of a solid subjected to forces [45]. Mooney-Rivlin model is a continuum mechanics model to study deformation of a hyperelastic solid. The Mooney-Rivlin is an update of the Neo-Hookean model and typically comes in two parameter, three parameter, five parameter or nine parameter [46]. The two parameter model is typically used for single curvature (no inflection points) materials in their stress-strain curve models. Five parameter and nine parameter forms are used if there is one or two inflection points in the material stress-strain curve models. This is shown in the figure 5 (a)-(c).
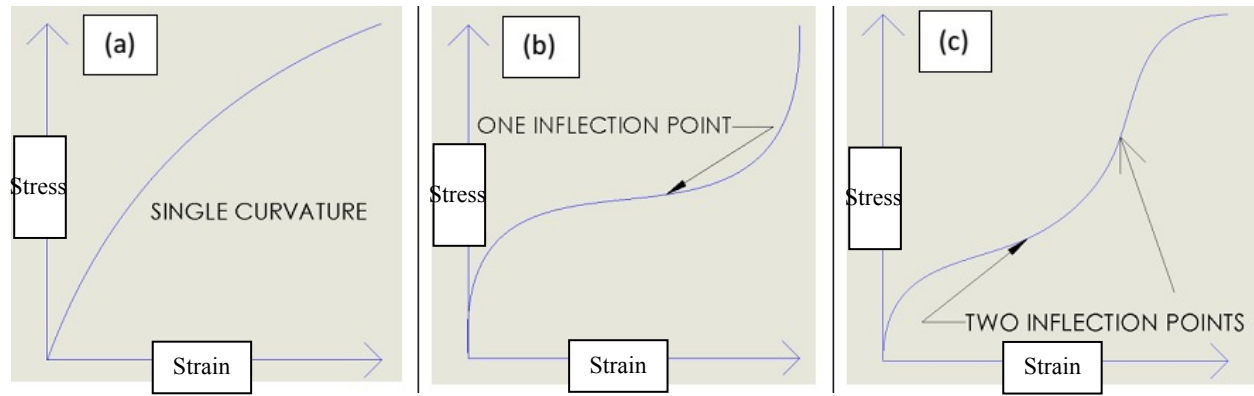

Figure 5. General hyperelastic material stress-strain curves (a) single curvature, (b) one inflection point and (c) two inflection points.

The two parametric form of Mooney-Rivlin model [48] is given by:

$$W = C_{10}(I_1 - 3) + C_{01}(I_2 - 3) + \frac{K}{2}(J - 1)^2 \tag{1}$$

Where C_{10} and C_{01} are constants derived from curve of the experimentally measured stress-strain of the material. I_1 and I_2 are the first and second invariant of the unimodular component of the left Cauchy-Green deformation tensor. J is the determent of deformation gradient F, and K is the distortional response.

We used the two parametric form of Mooney-Rivlin model for the analysis. The silicone material constants C_{10} and C_{01} were provided to the finite element analysis simulator using practical values. C_{10} and C_{01} were taken as 1 and 0.9 respectively from the experimental data published by Shergold et al. [47]. We used ABAQUS 6.13 as our Finite Element Analysis (FEA) simulator.

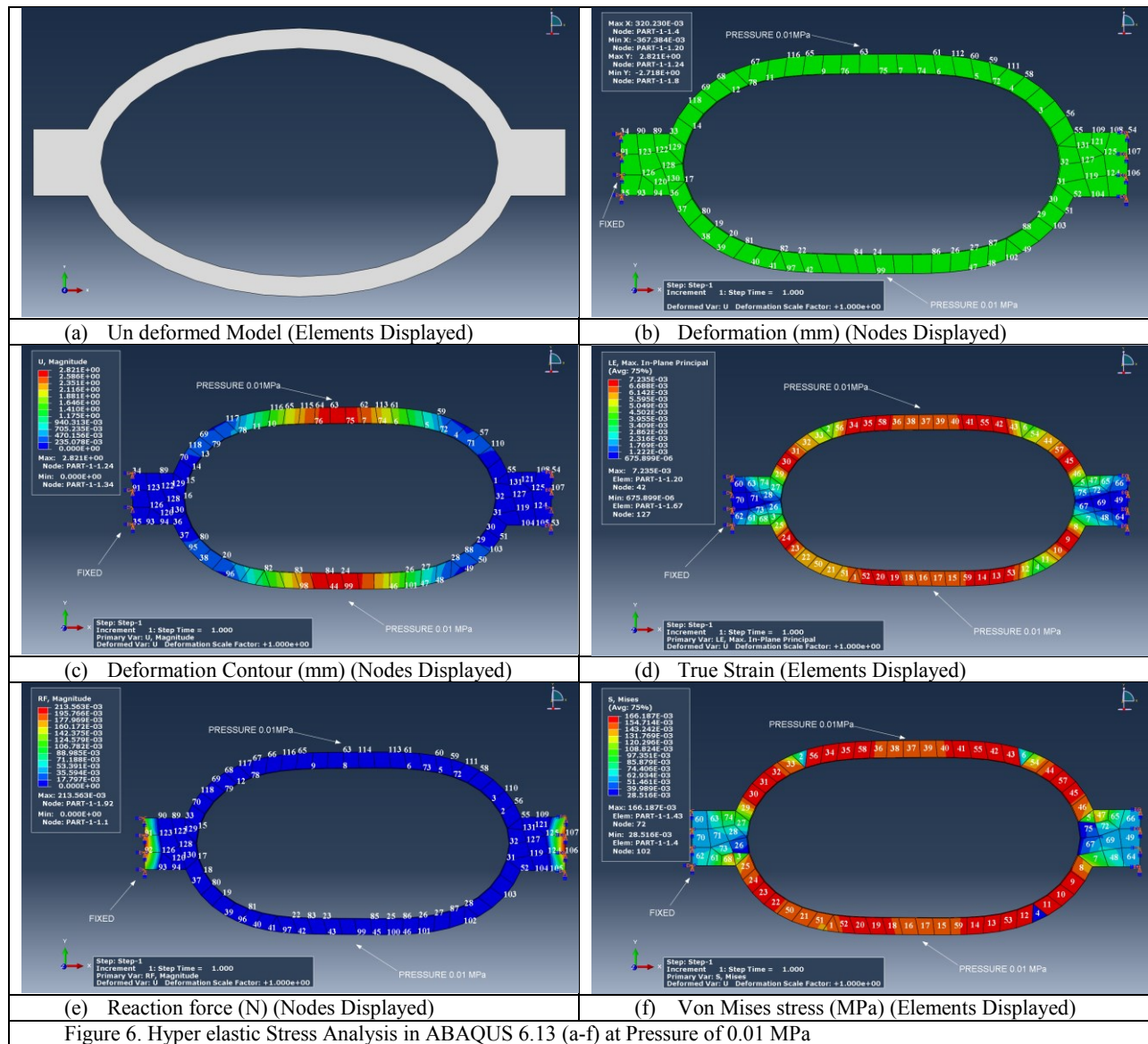| (a) Un deformed Model (Elements Displayed)	(b) Deformation (mm) (Nodes Displayed)
(c) Deformation Contour (mm) (Nodes Displayed)	(d) True Strain (Elements Displayed)
(e) Reaction force (N) (Nodes Displayed)	(f) Von Mises stress (MPa) (Elements Displayed)

Figure 6. Hyper elastic Stress Analysis in ABAQUS 6.13 (a-f) at Pressure of 0.01 MPa

The finite element analysis results are shown in Fig. 6. All the simulations were conducted using ABAQUS 6.13. The un-deformed model is shown in figure 6(a) depicting the center cross-section of the heart which has highest area. The cross-section was designed as a surface with surrounding faces to exact dimension of the prototype. The rectangular projections on the side were set to be the fixed in the model and also to hold the SMAs in position. The expected deformations of the SMAs are in the tangential direction of curved model as the SMAs are wounded around the curved surface of the model. The applied load on the model was a uniform pressure acting inward to the outer surface which will eventually reduce the volume of the model and pump the liquid out as desired. So we considered the resultant uniform pressure for the simulation. The pressure load was varied from 0.001 MPa to 0.01 MPa. The analysis is not conducted beyond 0.01 MPa as the deformation is too large for ABAQUS to numerically calculate due the hyperelastic property of the material and the simulation failed. The boundary condition used for the simulation was given by fixing the two extreme sides of the rectangular projections as shown in Figure 5 (b)-(f). The messing size used was 3 with the free Quad-dominated element shape which created 75 elements. Figure 5 (b) and (c) show the contour plot of the resultant deformation of the model after the simulation with maximum and minimum x axis and y axis at applied pressure of 0.01 MPa. The maximum deformation in x axis is 0.32 mm at node

4 and the minimum deformation in x axis is -0.367mm at node 20, the negative sign depicts the opposite direction. The maximum deformation in y axis is 2.821 mm at node 24 and the minimum deformation is -2.71 mm at node 8. The minimum resultant deformation is 0 mm at node 34(fixed end) as seen in figure 5 (c). Figure 5 (d) shows the maximum in plane principal true strain of average of 75% of all the elements in the contour deformed model with the maximum and minimum values 7.235×10^{-3} at element 20 and node 42 and 675.9×10^{-6} at element 67 and node 127 respectively. Figure 5 (e) shows the resultant reaction force of all the elements in the contour deformed model with the maximum and minimum values 213.563×10^{-3} N at node 92(fixed end) and 0 N at node 1 respectively. Figure 5 (f) shows the maximum Von Mises stress of average of 75% of all the elements in the contour deformed model with the maximum and minimum values 167.187×10^{-3} MPa at element 43(diagonal axis of the ellipse) and node 72 and 28.516×10^{-3} MPa at element 4 and node 102 respectively.
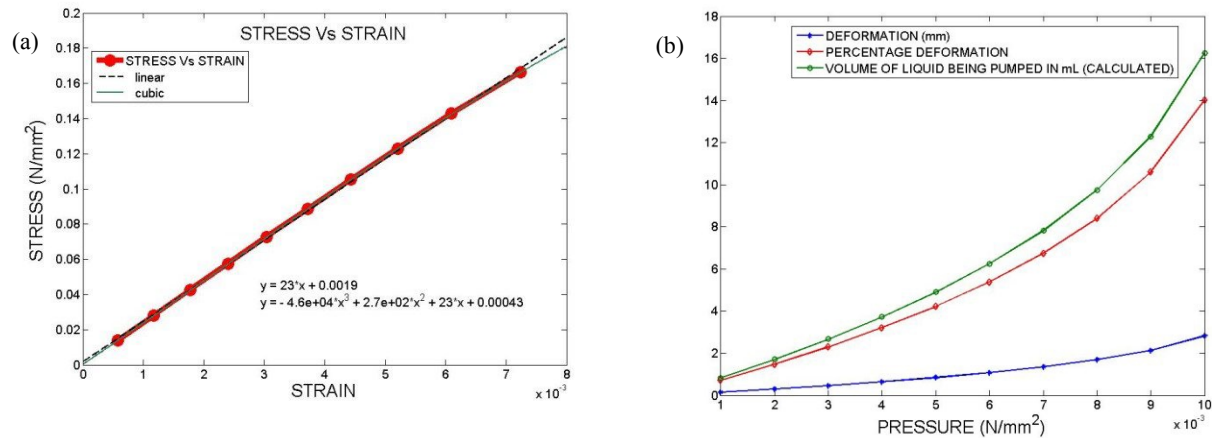

Figure 7. FEM simulation results plotted in MATLAB 2013b (a) Stress Vs Strain and (b) Pressure Vs (Deformation, % deformation and volume of liquid being pumped in mL (calculated)) on one side of the model

Figure 6 (a) shows the stress vs strain graph of the simulation obtained by varying pressure from 0.001 MPa to 0.01 MPa. The stress-strain curve shown in figure 6 is a linear relationship for the pressure considered. We can clearly see that figure 6 (a) and figure 3 (a) of the two parameter Mooney-Rivlin single curvature are similar as expected. The deformation analysis at the maximum possible pressure of 0.01 MPa was used to calculate the percentage deformation and provided approximately 14% on one side of the pressured model. Using this percentage deformation and integrating to the whole 3D model assuming that the deformation is uniform and constant all through the body on both sides, we obtained the reduction of volume in the model due to compression. It was found out that the volume of liquid as 2 x16.26 = 32.52 mm³ or 32.52 mL which is sufficient to clearly fill the cheeks of a humanoid with colored liquid (used as a blood). The actual pressure exerted by the SMAs will be much higher than the maximum pressure used in the simulation. This depends on directly on the length of SMA and maximum 4% deformation at maximum power conditions. The simulation results are in the range of experimental results and are in hyperelastic deformation neglecting hydrodynamic losses and inertial losses which can impact the performance of the actual pump.

3.3 Flow Analysis

The flow simulation was done in SolidWorks 2014 using its FloWorks 2014 (Dassault Systemes, France) flow simulator. The inlet and outlet pressure conditions were taken from the results presented by Hayward et al. [48], the maximum pressure a regular small scale syringes can produce. From the previous hyperelastic simulation conducted at maximum possible load pressure of 0.01 MPa, we calculated the maximum volume that can be pumped and obtained approximately 32.52 mL. From the results of Hayward et al., we best estimated the volume displaced assuming the heart model has similar pressure drop as the syringe and used a maximum pressure drop of approximately 32 psi. Therefore, we set the inlet pressure at 43 psi and varied the outlet pressure from 11 psi, 17 psi, 23 psi, 29 psi and 35 psi to obtain different maximum velocities at five different pressure values. The analysis assumed that the robotic heart pump is already deformed due to actuation and the flow analysis was carried out assuming constant volume at certain period of time. This estimation was done mainly to see the variation of the

velocities at different pressures and to see the flow path of the liquid inside the heart model using practical values. The simulation was done at temperature of 68.09 ºF (room temperature). Figure 8(a) and (b) show the volume of fluid (blue color), and the inlet and outlet of the heart model respectively.
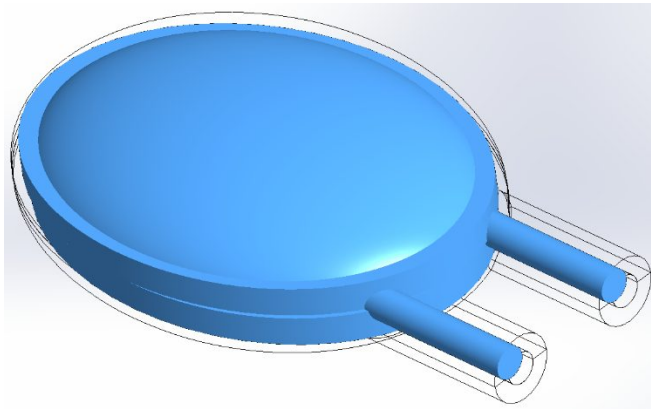

Figure 8. (a) Volume of the fluid inside the heart model during Flow Simulation = 116 mm³ or 116 mL
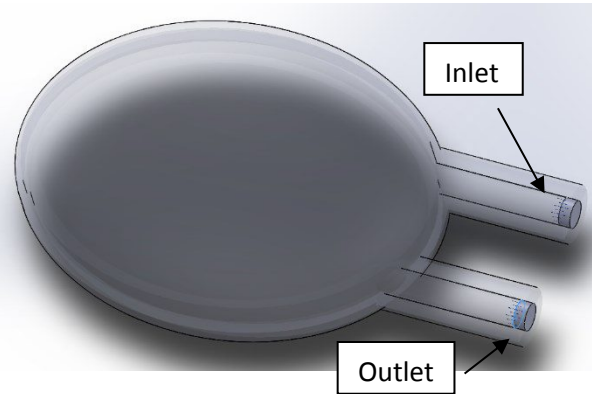

Figure 8(b). Shows the inlet and outlet valves of the flow simulation

Figure 9 shows the simulation results of the maximum velocity of the fluid with respect to the variation of pressure drop. We can clearly see that after a certain increase in pressure drop the curve becomes more linear. The values of the pressure drop were taken at five data points (8psi to 32psi) and the maximum velocities were in the range of 350-700 in/sec. Figure 10 shows the flow simulation at maximum pressure drop of 32 psi (where inlet pressure is 43 psi and outlet pressure is 11 psi) and the corresponding maximum velocity is 691.6 in/sec. The main purpose of the flow simulation is to observe how the fluid flows through the robotic heart chamber. A metaphysics simulation which can perform flow with deformation would give more accurate results but these results still show us a very clear concept on the nature of the fluid inside the artificial heart proposed in this paper functions. The screen shot of the flow at 1, 1.5 and 2 seconds are shown in figure 10 where the fluid flow in within the surface and continued to circulate inside the chamber and finally exits. It can be seen that the central portion has less velocity.
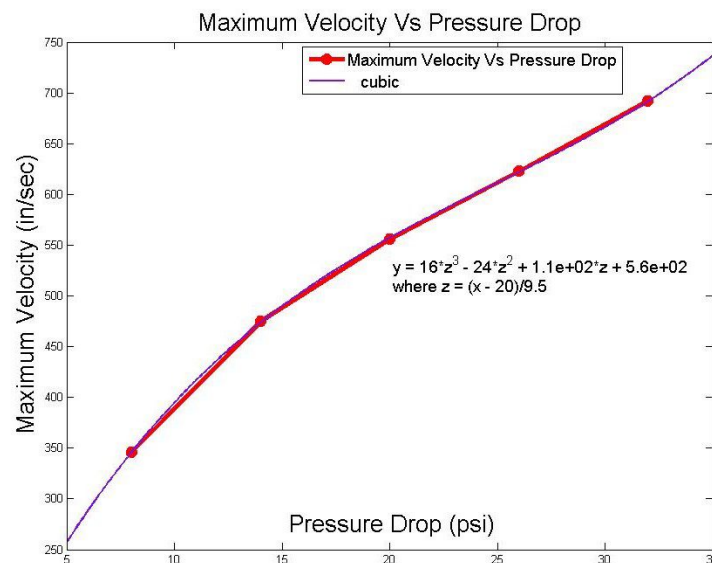

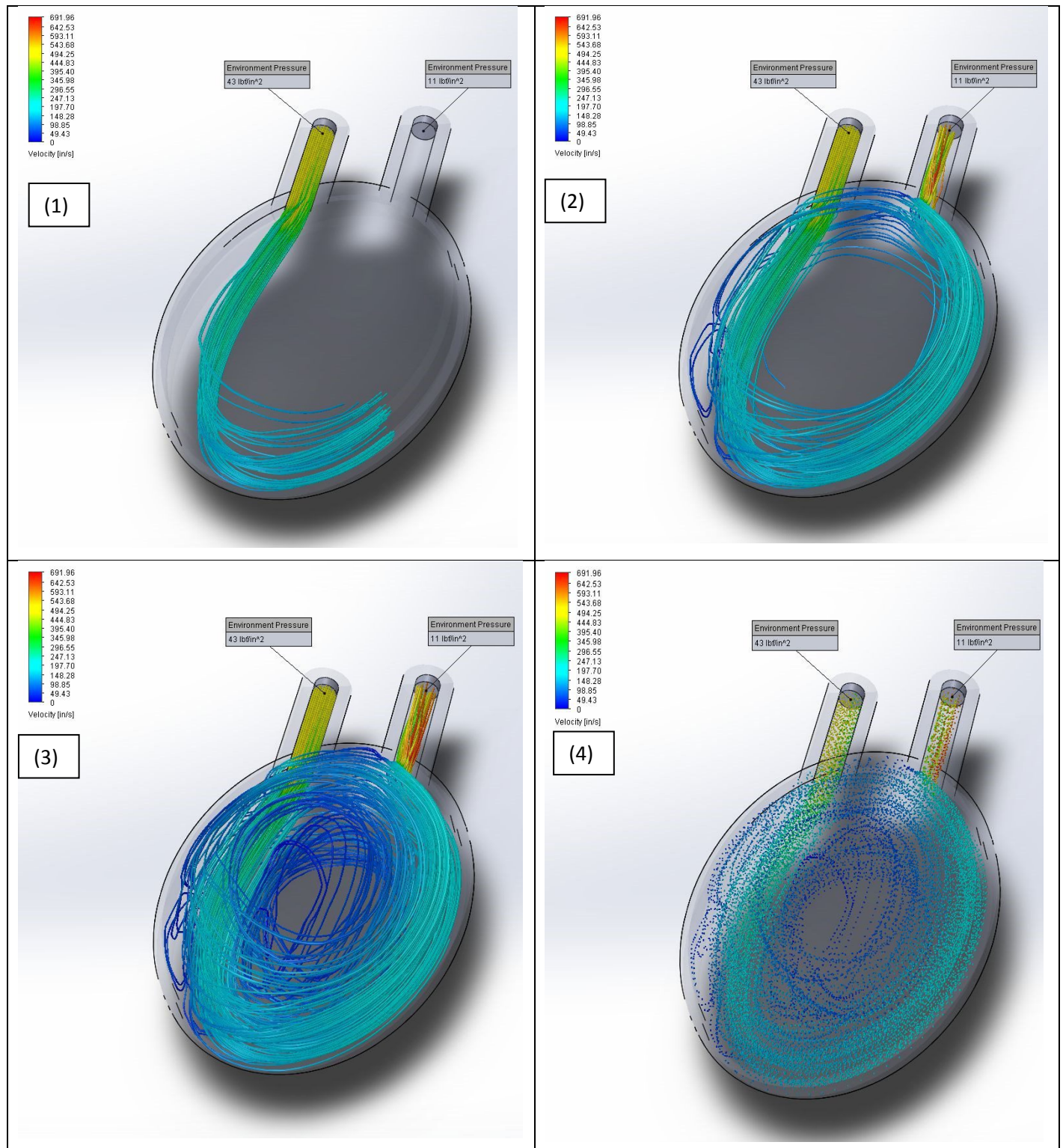Figure 9. Plot of Maximum Velocity Vs Pressure Drop

Figure 10. Flow analysis of computer aided design of the artificial heart in SolidWorks (1-3) in pipes in 1,1.5 and 2 seconds of simulation run respectively and (4) in balls for the maximum pressure drop of 32 psi (where inlet pressure is 43 psi and outlet pressure is 11 psi)

4. EXPERIMENT RESULT AND DISCUSSION

4.1 Heart pumping test

In this section, we describe the experimental setup to test the behavior of the artificial heart. The experimental setup is comprised of power supply (Topward 6306D) and National Instruments data acquisition system (NI 9201) with a computer interface and LabVIEW program. Schematic diagram of experimental setup is shown in Figure 11.The heart was wrapped with the SMA fibers whose ring terminals were anchored to the surrounding clamp. The terminals of the SMA wires were connected to the power supply. The heart was filled with water mixed with red
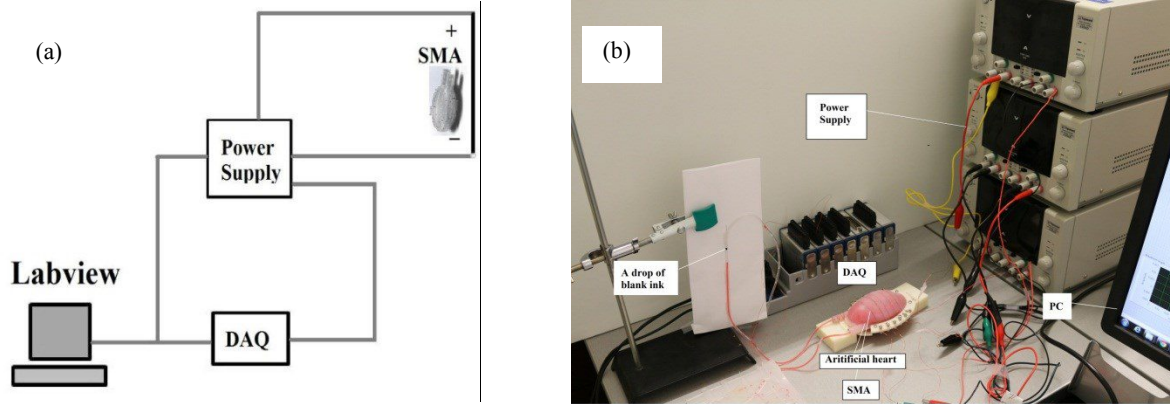

Figure 11. (a) Schematic diagram of the experimental setup, and (b) picture of the laboratory experimental setup

ink. Two small blocks was designed to support the clamp so that the artificial heart was unsupported to get realistic deformation for heart pumping testing. Two transparent plastic tubes were attached to the inlet and outlet ports. A drop of black ink was ejected into the transparent tube connecting to the outlet port for tracking purpose using image processing in MatLab^{TM}. A canon camera was placed in front of the black ink to record its displacement. Once all preparation has been made, the tests were conducted by activating the SMA actuators.
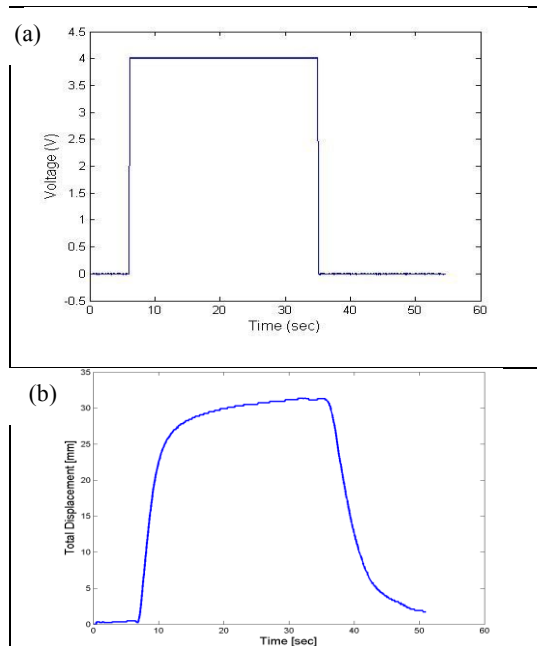
The artificial heart operates as follows: power is supplied to the terminal of the SMA fibers; the SMA fibers are heated by the electric current and the rise in temperature cause them to undergo phase transformation, leading the contraction in length. The soft artificial heart is compressed due to the contraction of the SMA fibers. The water inside of the artificial heart is forced outwards through the hollow body of the heart. Meanwhile the camera records the displacement of the drop of black ink to track the water flow in the tube. Once the electric current is removed from the SMA fibers, the soft heart returns back to the rest position with the help of the 'recovery force' provided by the sponge.

The characteristics of the employed Flexinol wires are given in table 1. Since two different SMA wires were used in robotic heart, the actuation of SMAs was performed as follows. The SMA fibers (130 μm in diameter) were supplied with a current of 310 mA at 4.0 V, and the SMA fibers (200 μm in diameter) were supplied with a current of 520 mA at 3.0 V. The artificial heart was compressed upon the SMA fibers' contraction. The results of this test are illustrated in figure 12 and 13 in terms of the displacement of the drop of black ink and the deformation of the

Figure 12. (a) Voltage applied to the SMA fibers(130 μm in diameter) and (b) the displacement of the drop of the black ink.

heart. Figure 12(a) shows only the voltage supplied to the SMA fibers whose diameter is 130 μm. Figure 12(b) show the corresponding displacement of the drop of the black ink in the tube under the action of the SMA fibers. It can be observed in this figure that in the rising stage, the displacement has a sharp increase at the beginning, indicating that

the artificial heart is undergoing sudden deformation. Comparing the raising edge of displacement with the falling edge of displacement, it can also be noticed that it takes much longer time for the ink to attain a steady position during the raising stage than the falling stage. Figure 13 shows the snap shots of the deformed artificial heart. It was noted here that the far left SMA fiber was not actuated. We compared the deformed shape and undeformed shape of the artificial heart and sketched the outline of the artificial heart to calculate the deformation. The deformation of the seven regions located in Fig.13(c) was magnified and the nut was used as scale. The displacement of these regions marked from No.1 to No.7 are 0.468mm, 0.355mm, 0.062mm, 0.075mm, 0.190mm, 0.600mm, 0.014mm and 0.369mm. It was observed that the force generated by SMA fibers had a local deformation on the artificial heart. Due to the liquid flow and the hyperelastic characteristic of the silicone, it can be noticed that the top and bottom end of the artificial heart were expanded.

Table 1. Actuator parameters of SMA wires

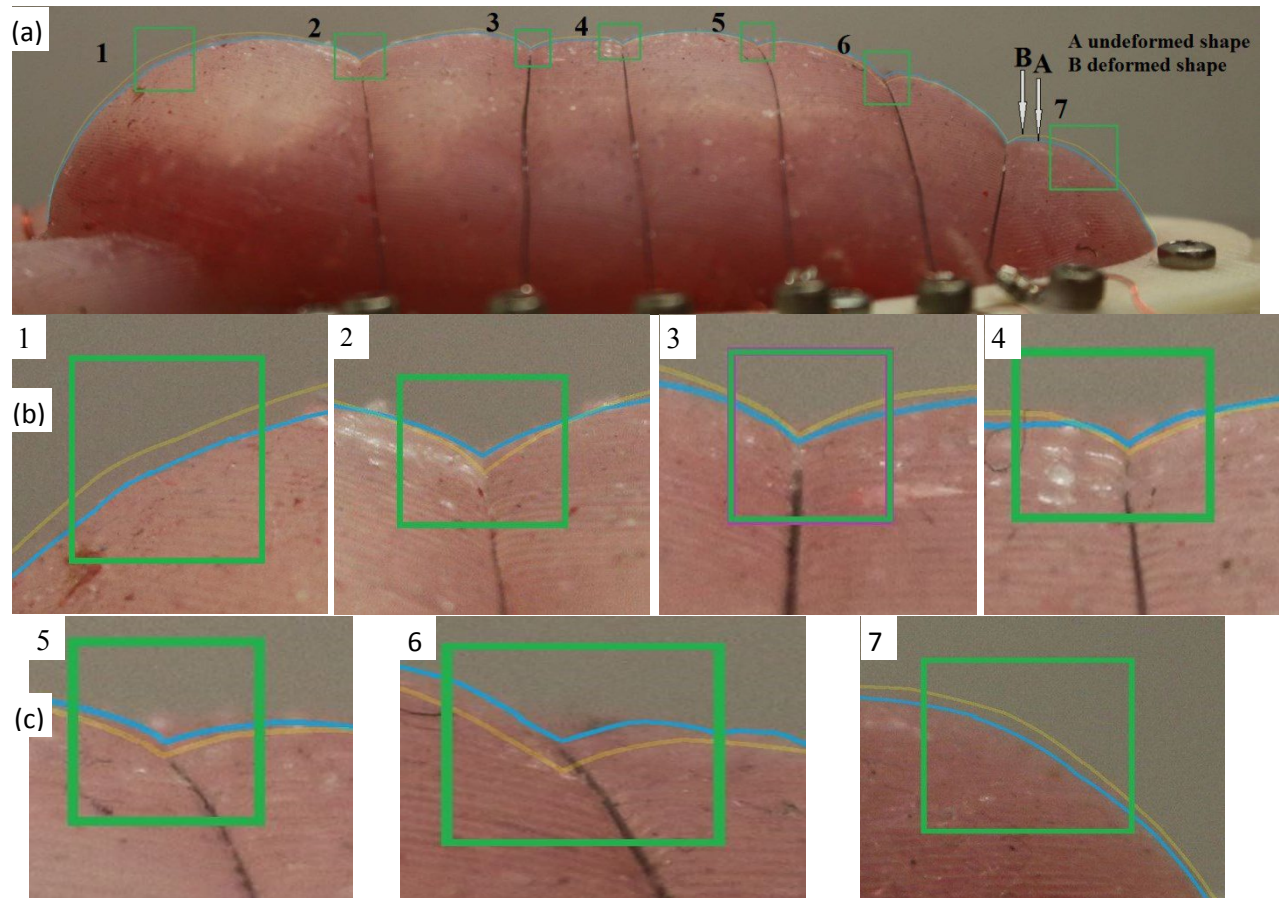| Actuators parameters	Flexion wires	
Diameter(μm)	130	200
Max force(grams)	223	570
Resistance (Ω/m)	75	29
Strain	3%-5%	3%-5%
Current(mA)	320	660

Figure 13. (a)deformation of the artificial heart, and (b) &(c) magnified views of the deformation(No.1~No.7)

In order to gain a better performance of the artificial heart, further experiment was carried out to compare the artificial heart pumping effect. In the previous test (also shown in Fig 14(a)), test 1, it was shown that the contraction of SMA fibers was only caused localized deformation of the heart. In another test, test 2, the artificial was covered with the tapes to distribute the force generated by SMA fibers uniformly on the heart body (Fig.14 (b)). These two experiments were carried out by applying the same voltage to the SMA fibers. The displacement of the drop of blank ink within the outlet pipe was recorded and the results are shown in figure 15, indicating that the one with tapes had much better pumping effect than that a bare SMA on the silicone. The magnitude of total displacement of the droplet was 30 mm and 75 mm for test 1 and test 2 respectively as shown in figure 15.
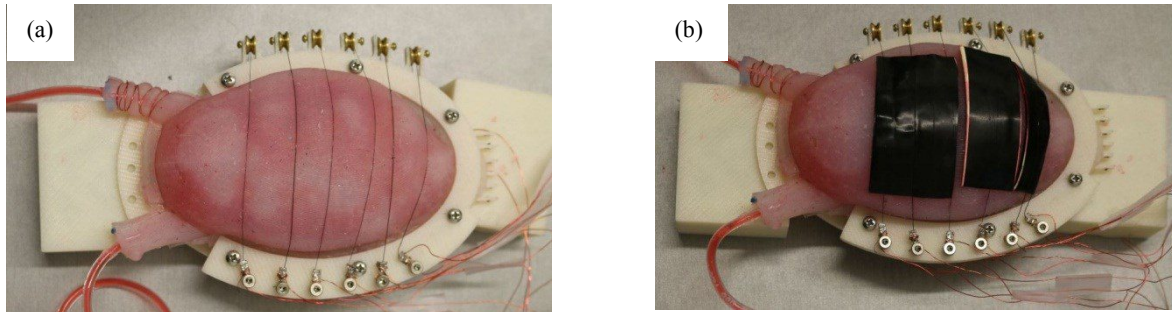

Figure 14. (a) Test 1:SMA fibers contact with artificial heart directly and (b) Test2: Artificial heart covered with tape.
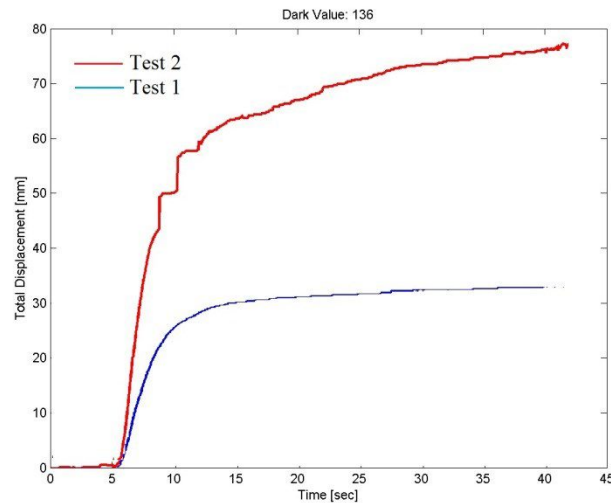

Figure 15. Displacement of the drop of blank ink using a tape on the silicone and without

5. APPLICATIONS

Facial color change is an effective nonverbal communication and it plays a significant role in expressing oneself. Human heart plays a vital role in change of facial color as the flow of blood is regulated by the heart to face. A study showed that humans connect facial expressions with certain colors [8]. The study showed anger and happiness are connected to the color red as in naturally we blush for happiness, anger and embarrassment and the color green is connected to disgust and sickness. Naturally these colors are exhibited in humans due to sudden variation in blood pumping to face from heart due to emotional changes experienced which are controlled by the brain. The prominent area of application is in humanoid robots with facial expressions (HRwFE). If these robots are provided with the ability to change colors while actuating their face muscles, better emotional expressions can be added obtained. This has an application in medical studies through the use of humanoids. Figure 16 illustrates the basic idea of the application in humanoids. The general idea is to implement the artificial heart to pump a blood like fluid (red color water) to the humanoid robot face to mimic the human facial color changes. In figure 16, a transparent tube

embedded in the silicone layer (much smaller size) was made and the inlet was connected to the robotic heart. As the SMA actuators are activated the blood like fluid came out and passing through the channels. Although the spacing between the pipes is not sufficient to make significant change in the color, the concept is applicable to use in humanoid robots. Particularly, the cheeks of a humanoid are an ideal area to implement on humanoid robot face. When the colorized water reaches the specific areas of the face, it will enable the robot to making facial expression in an effective nonverbal way.
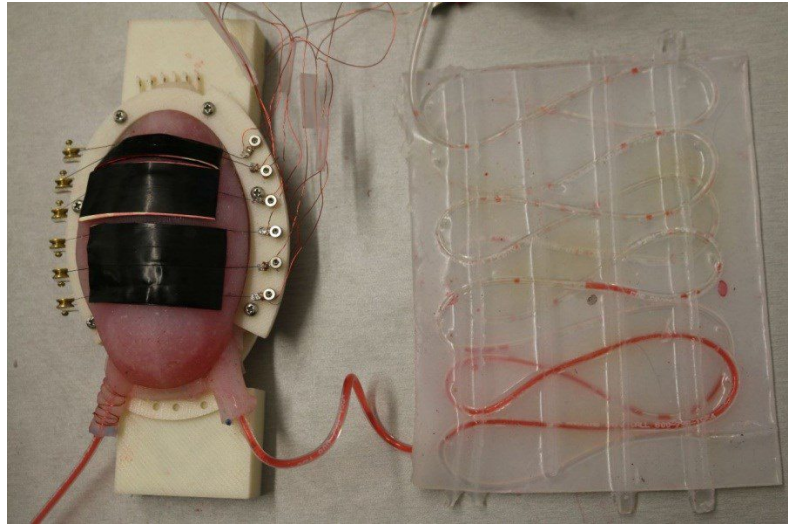

Figure 16. The transparent silicone layer embedded with tube for demonstrating the facial color change

6. CONCLUSION

The design and fabrication of a soft artificial heart for humanoid robot was presented in this paper using silicone elastomer and shape memory alloy actuators. The deformation behavior of the heart model was studied under different pressures using finite element analysis. Mooney-Rivlin model was used to predict the deformation of the silicone material that was used to make the artificial heart. Hyperelastic deformation behavior was observed in the simulation results that are associated with the volume of fluid pumped out. Flow analysis was also performed to understand how the fluid flows through the hollow body of the artificial heart. The displacement of a drop of black ink was used to characterize the pumping action of the artificial heart. In addition, the deformation of the artificial heart was studied by applying appropriate voltage. The results showed that direct contact between SMA fibers and artificial heart can pump the water out from the heart, but caused localized deformation. A better performance of the artificial heart was obtained by covering the heart with tape and uniformly distributing the force generated by SMA fibers through the body of the heart. We envisage that the robotic heart can pump a blood-like fluid to parts of the robot such as the face to simulate someone blushing or when someone is angry by the use of elastomeric substrates and certain features for the transport of fluids. This study is not only useful in humanoids but also applicable in the medical fields. In a nutshell, the study will help us to develop a better robotic heart for biomedical applications.

REFERENCES

[1]   A. Coghlan, "Life savers: a history of the artificial heart," *New Scientist* 220(2945), 26-27 (2013)
[2]   A. H. Association, *American Heart Association's Complete Guide to Heart Health: American Heart Association*, Pocket Books (1996).
[3]   T. Yamada and T. Watanabe, "Effects of facial color on virtual facial image synthesis for dynamic facial color and expression under laughing emotion," in *Robot and Human Interactive Communication, 2004. ROMAN 2004. 13th IEEE International Workshop on*, pp. 341-346, IEEE (2004).
[4]   H. D. Critchley, P. Rotshtein, Y. Nagai, J. O'Doherty, C. J. Mathias and R. J. Dolan, "Activity in the human brain predicting differential heart rate responses to emotional facial expressions," *Neuroimage* 24(3), 751-762 (2005)
[5]   D. Shearn, E. Bergman, K. Hill, A. Abel and L. Hinds, "Facial coloration and temperature responses in blushing," *Psychophysiology* 27(6), 687-693 (1990)
[6]   C. Darwin, *The expression of the emotions in man and animals*, Oxford University Press (1998).
[7]   M. Lewis, J. M. Haviland-Jones and L. F. Barrett, *Handbook of Emotions*, Guilford Publications (2010).

[8]   O. da Pos and P. Green-Armytage, "Facial expressions, colours and basic emotions," *JAIC-Journal of the International Colour Association* 1((2012)

[9]   J. K. Wilkin, "Why is flushing limited to a mostly facial cutaneous distribution?," *Journal of the American Academy of Dermatology* 19(2), 309-313 (1988)

[10]   N. A. Gray Jr and C. H. Selzman, "Current status of the total artificial heart," *American heart journal* 152(1), 4-10 (2006)

[11]   L. Joyce, W. DeVries, W. Hastings, D. Olsen, R. Jarvik and W. Kolff, "Response of the human body to the first permanent implant of the Jarvik-7 total artificial heart," *ASAIO Journal* 29(81&hyhen (1983)

[12]   W. C. DeVries, "The permanent artificial heart: Four case reports," *Jama* 259(6), 849-859 (1988)

[13]   F. Arabia, J. Copeland, R. Smith, M. Banchy, B. Foy, R. Kormos, A. Tector, J. Long, W. Dembitsky and M. Carrier, "CardioWest total artificial heart: a retrospective controlled study," *ARTIFICIAL ORGANS-OHIO-* 23(204-207 (1999)

[14]   D. A. Cooley, D. Liotta, G. L. Hallman, R. D. Bloodwell, R. D. Leachman and J. D. Milam, "Orthotopic cardiac prosthesis for two-staged cardiac replacement," *The American journal of cardiology* 24(5), 723-730 (1969)

[15]   D. Pennington, K. Kanter, L. McBride, G. Kaiser, H. Barner, L. Miller, K. Naunheim, A. Fiore and V. Willman, "Seven years' experience with the Pierce-Donachy ventricular assist device," *The Journal of thoracic and cardiovascular surgery* 96(6), 901-911 (1988)

[16]   M. Kobayashi, D. J. Horvath, N. Mielke, A. Shiose, B. Kuban, M. Goodin, K. Fukamachi and L. A. Golding, "Progress on the Design and Development of the Continuous-Flow Total Artificial Heart," *Artificial organs* 36(8), 705-713 (2012)

[17]   B. Zhang, T. Masuzawa, E. Tatsumi, Y. Taenaka, C. Uyama, H. Takano and M. Takamiya, "Three-Dimensional Thoracic Modeling for an Anatomical Compatibility Study of the Implantable Total Artificial Heart," *Artificial organs* 23(3), 229-234 (1999)

[18]   S. Takatani, M. Shiono, T. Sasaki, I. Sakuma, J. Glueck, M. Sekela, C. NOON, Y. Nose and M. DeBakey, "A unique, efficient, implantable, electromechanical, total artificial heart," *ASAIO Journal* 37(3), M238-M239 (1991)

[19]   P. Walters, A. Lewis, A. Stinchcombe, R. Stephenson and I. Ieropoulos, "Artificial heartbeat: design and fabrication of a biologically inspired pump," *Bioinspiration & biomimetics* 8(4), 046012 (2013)

[20]   E. Roche, A. Menz, P. Hiremath, N. Vasilyev, D. Mooney and C. Walsh, "Design of an anatomically accurate, multi-material, patient-specific cardiac simulator with sensing and controls,"

[21]   Y. Tadesse, "Electroactive polymer and shape memory alloy actuators in biomimetics and humanoids," in *SPIE Smart Structures and Materials+ Nondestructive Evaluation and Health Monitoring*, pp. 868709-868709-868712, International Society for Optics and Photonics (2013).

[22]   Y. Tadesse, D. Hong and S. Priya, "Twelve degree of freedom baby humanoid head using shape memory alloy actuators," *Journal of Mechanisms and Robotics* 3(1), 011008 (2011)

[23]   Y. Tadesse, "Actuation Technologies for Humanoid Robots with Facial Expressions (HRwFE)," *Transaction on Control and Mechanical Systems* 2(7), (2013)

[24]   Y. Tadesse, "Actuation technologies suitable for humanoid robots," in *ASME 2012 International Mechanical Engineering Congress and Exposition*, pp. 1-10, American Society of Mechanical Engineers (2012).

[25]   M. D. Pierce and S. A. Mascaro, "A biologically inspired wet shape memory alloy actuated robotic pump," *Mechatronics, IEEE/ASME Transactions on* 18(2), 536-546 (2013)

[26]   Y. Suzuki, K. Daitoku, M. Minakawa, K. Fukui and I. Fukuda, "Dynamic cardiomyoplasty using artificial muscle," *Journal of Artificial Organs* 11(3), 160-162 (2008)

[27]   P. Sawyer, M. Page, L. Baseliust, C. McCool, E. Lester, B. Stanczewski, S. Srinivasan and N. Ramasamy, "Further study of nitinol wire as contractile artificial muscle for an artificial heart," *Cardiovascular diseases* 3(1), 65 (1976)

[28]   Y. Shiraishi, T. Yambe, Y. Saijo, F. Sato, A. Tanaka, M. Yoshizawa, T. Sugai, R. Sakata, Y. Luo and Y. Park, "Sensorless control for a sophisticated artificial myocardial contraction by using shape memory alloy fibre," in *Engineering in Medicine and Biology Society, 2008. EMBS 2008. 30th Annual International Conference of the IEEE*, pp. 711-714, IEEE (2008).

[29]   Q. A. Acton, *Robotics—Advances in Research and Application: 2013 Edition*, ScholarlyEditions (2013).

[30] D. Hanson, "Exploring the aesthetic range for humanoid robots," in *Proceedings of the ICCS/CogSci-2006 long symposium: Toward social mechanisms of android science*, pp. 39-42, Citeseer (2006).

[31] K. Berns and J. Hirth, "Control of facial expressions of the humanoid robot head ROMAN," in *Intelligent Robots and Systems, 2006 IEEE/RSJ International Conference on*, pp. 3119-3124, IEEE (2006).

[32] J.-H. Oh, D. Hanson, W.-S. Kim, I. Y. Han, J.-Y. Kim and I.-W. Park, "Design of android type humanoid robot Albert HUBO," in *Intelligent Robots and Systems, 2006 IEEE/RSJ International Conference on*, pp. 1428-1433, IEEE (2006).

[33] D. Hanson, R. Bergs, Y. Tadesse, V. White and S. Priya, "Enhancement of EAP actuated facial expressions by designed chamber geometry in elastomers," in *Smart Structures and Materials*, pp. 616806-616806-616809, International Society for Optics and Photonics (2006).

[34] G. Trovato, T. Kishi, N. Endo, K. Hashimoto and A. Takanishi, "Development of facial expressions generator for emotion expressive humanoid robot," in *Humanoid Robots (Humanoids), 2012 12th IEEE-RAS International Conference on*, pp. 303-308, IEEE (2012).

[35] T. Hashimoto, S. Hitramatsu, T. Tsuji and H. Kobayashi, "Development of the face robot SAYA for rich facial expressions," in *SICE-ICASE, 2006. International Joint Conference*, pp. 5423-5428, IEEE (2006).

[36] W. Weiguo, M. Qingmei and W. Yu, "Development of the humanoid head portrait robot system with flexible face and expression," in *Robotics and Biomimetics, 2004. ROBIO 2004. IEEE International Conference on*, pp. 757-762, IEEE (2004).

[37] S. Nishio, H. Ishiguro and N. Hagita, "Geminoid: Teleoperated android of an existing person," *Humanoid robots-new developments. I-Tech* 14((2007)

[38] H. Miwa, T. Umetsu, A. Takanishi and H. Takanohu, "Human-like robot head that has olfactory sensation and facial color expression," in *Robotics and Automation, 2001. Proceedings 2001 ICRA. IEEE International Conference on*, pp. 459-464, IEEE (2001).

[39] W. Zhiliang, L. Yaofeng and J. Xiao, "The research of the humanoid robot with facial expressions for emotional interaction," in *Intelligent Networks and Intelligent Systems, 2008. ICINIS'08. First International Conference on*, pp. 416-420, IEEE (2008).

[40] Y. Tadesse, S. Priya, H. Stephanou, D. Popa and D. Hanson, "Piezoelectric actuation and sensing for facial robotics," *Ferroelectrics* 345(1), 13-25 (2006)

[41] Y. Tadesse, K. Subbarao and S. Priya, "Realizing a humanoid neck with serial chain four-bar mechanism," *Journal of Intelligent Material Systems and Structures* 21(12), 1169-1191 (2010)

[42] " Heart," in *Wikipedia*, Wikimedia Foundation.

[43] M. Mooney, "A theory of large elastic deformation," *Journal of applied physics* 11(9), 582-592 (2004)

[44] R. Rivlin, "Large elastic deformations of isotropic materials. IV. Further developments of the general theory," *Philosophical Transactions of the Royal Society of London. Series A, Mathematical and Physical Sciences* 241(835), 379-397 (1948)

[45] E. W. V. Chaves, *Continuum Mechanics: Fundamental Concepts and Constitutive Equations*, International Center for Numerical Methods in Engineering (CIMNE) (2013).

[46] B. J. M. Donald, *Practical Stress Analysis with Finite Elements*, Glasnevin (2007).

[47] O. A. Shergold, N. A. Fleck and D. Radford, "The uniaxial stress versus strain response of pig skin and silicone rubber at low and high strain rates," *International Journal of Impact Engineering* 32(9), 1384-1402 (2006)

[48] W. Hayward, L. J. Haseler, L. Kettwich, A. Michael, W. Sibbitt Jr and A. Bankhurst, "Pressure generated by syringes: implications for hydrodissection and injection of dense connective tissue lesions," *Scandinavian journal of rheumatology* 40(5), 379-382 (2011)